

CLOSED CORONAL STRUCTURES. VI. FAR-ULTRAVIOLET AND X-RAY EMISSION  
FROM ACTIVE LATE-TYPE STARS AND THE APPLICABILITY OF  
CORONAL LOOP MODELSMARK S. GIAMPAPA,<sup>1,4</sup> LEON GOLUB,<sup>2,4</sup> GIOVANNI PERES,<sup>2,3</sup> SALVATORE SERIO,<sup>2,3</sup>  
AND GIUSEPPE S. VAIANA<sup>2,3,4</sup>*Received 1983 September 23; accepted 1984 August 17*

## ABSTRACT

We present far-ultraviolet line fluxes of prominent transition region emission lines, as obtained with the *International Ultraviolet Explorer* satellite, for a sample of solar-type stars. We combine the ultraviolet observations with existing soft X-ray measurements obtained by the *Einstein Observatory* (HEAO 2). We utilize the resulting data set and a new coronal loop model numerical code developed at the Harvard-Smithsonian Center for Astrophysics to perform a preliminary investigation of the applicability of coronal loop models to solar-type stars. In a few cases, reasonable agreement between the predictions of single-component, coronal loop model atmospheres and the observational data is achieved for a relatively well-defined, plausible range of values in the pressure-filling factor ( $p, f$ ) plane. In general, however, we find that the addition of non-simultaneous ultraviolet observations to a previously acquired soft X-ray data set does not provide a sufficient constraint on the range of possible loop filling factors and pressures for loop model atmospheres that may be producing the observed X-ray and transition region emissions. We discuss the origins of the discrepancies between the model results and the observations within the context of (1) stellar variability, (2) multiple coronal components, and (3) the presence of relatively low temperature loops that give rise to far-ultraviolet emission but not to coronal X-ray emission. We suggest on the basis of the results presented in this investigation that in order to verify the applicability of coronal loop models to solar-type stars, *simultaneous* far-ultraviolet and moderate spectral resolution X-ray observations will eventually have to be obtained.

*Subject headings:* stars: coronae — stars: late-type — ultraviolet: spectra

## I. INTRODUCTION

The atmosphere of the Sun exhibits a variety of structural inhomogeneities that are defined by magnetic field configurations. These magnetic field structures are often observed to coincide with sites of intense chromospheric and coronal emission (e.g., see Van Speybroeck, Krieger, and Vaiana 1970) where the degree of emission enhancement is empirically related to the open or closed nature of the magnetic field configuration and the associated nonradiative heating mechanism that is operative (e.g., see Rosner *et al.* 1978; Ionson 1978). We now recognize these atmospheric inhomogeneities as a *fundamental* property of the solar outer atmosphere (see the review by Vaiana and Rosner 1978). Magnetic field configurations that control atmospheric thermal inhomogeneities are especially evident in the solar corona, which is characterized by open and closed coronal loop structures. The investigation of these structures included the delineation of the physical structure of open (Rosner and Vaiana 1977) and closed field regions in the solar corona, culminating in the development of scaling laws relating loop size, temperature, and pressure for coronal loops in hydrostatic equilibrium (Rosner, Tucker, and Vaiana 1978, hereafter RTV). The hydrostatic loop models have been generalized by Serio *et al.* (1981) and utilized by Pallavicini *et al.* (1981) for the analysis and interpretation of solar X-ray,

extreme ultraviolet, and radio observations. The results of these solar investigations may be applicable to stars given that the occurrence of stellar surface features similar to solar plage and sunspots is now well established (e.g., see Wilson 1978; Vaughan *et al.* 1981; Radick *et al.* 1983).

The existence of *stellar* surface inhomogeneities, analogous to solar surface features, provides compelling circumstantial evidence for the presence of stellar coronal magnetic field structures that are similar to solar coronal loops. Thus the analysis of stellar transition region and coronal emission within the context of solar coronal loop models is a natural extension of solar physics. Conversely, stellar observations provide the means of comparing the chromospheres and coronae of stars with varying levels of activity, thus enabling us to verify the applicability to solar-type stars of specific atmospheric scaling laws originally developed for the Sun. In this perspective the study of stellar atmospheres becomes an integral part of solar chromospheric and coronal physics.

The widespread occurrence of coronae among active, late-type stars (Vaiana *et al.* 1981; Pallavicini *et al.* 1981) has stimulated investigations of the hypothesis that the observed X-ray emission arises from structured loop atmospheres, similar to that of the solar corona, but at enhanced levels in terms of loop pressures, temperatures, lengths, and filling factors. In particular, Walter *et al.* (1980) explored the applicability of coronal loop models to explain the observed emission measures, pressures, temperatures, and variability exhibited by RS CVn systems, as deduced primarily from X-ray data. In addition, Swank *et al.* (1981) utilized the solid state spectrometer on board the *Einstein Observatory* (HEAO 2) to infer the presence of two-component X-ray emission from RS CVn systems.

<sup>1</sup> National Solar Observatory, National Optical Astronomy Observatories (NOAO). The NOAO is operated by the Association of Universities for Research in Astronomy, Inc., under contract to the National Science Foundation.

<sup>2</sup> Harvard-Smithsonian Center for Astrophysics.

<sup>3</sup> Istituto e Osservatorio Astronomico di Palermo, Italy.

<sup>4</sup> Guest Observer, *International Ultraviolet Explorer* Satellite Observatory.

More specifically, these investigators suggested that the coronae of RS CVn binaries are well described by an active, hot component ( $T \sim 10^7$  K) composed of compact, high-pressure ( $p > 10^2$  dynes  $\text{cm}^{-2}$ ) loops covering only small fractions of the stellar surfaces combined with a quiescent component characterized by temperatures  $T \sim 10^6$  K, pressure  $p \leq 10$  dynes  $\text{cm}^{-2}$ , and filling factors near unity.

Recently, Golub *et al.* (1982a) discussed the applicability of coronal loop models to more nearly solar-type stars in their examination of the detected X-ray emission from the  $\alpha$  Centauri system. These investigators emphasize that, without additional constraints, coronal loop models deduced solely on the basis of spatially unresolved stellar X-ray observations can only yield a locus of possible atmospheres in the coronal pressure-filling factor ( $p, f$ ) plane. Golub *et al.* (1982a) note, however, that the coronal filling factor of identical loops can be uniquely determined if the loop lengths are all equal to the local coronal pressure scale height. Finally, Walter, Gibson, and Basri (1983) simultaneously acquired X-ray, ultraviolet, and radio eclipse data for the RS CVn system AR Lacertae. In this way, these investigators were able to deduce geometrical scales that enabled them to determine more uniquely the coronal properties of this system. In particular, they inferred that the coronae must be composed of a large number ( $\sim 10^5$ – $10^6$ ) of magnetic loops to produce the observed emission. Moreover, the inferred pressures and densities were similar to those found in small solar flares.

In this study we present a unique extension of previous investigations of the applicability of solar coronal loop models as descriptions of stellar coronal and transition region emission (see also Schmitt *et al.* 1985). More specifically, we utilize observed far-ultraviolet line fluxes of prominent transition region emission lines, as obtained with the *International Ultraviolet Explorer (IUE)* satellite, combined with measurements of coronal soft X-ray emission, acquired by the *Einstein Observatory*, to construct semiempirical, single-component loop model atmospheres that best fit the aforementioned observations for a sample mainly composed of solar-type stars. In this way, we can ascertain the extent to which the addition of UV transition region observations to X-ray measurements can constrain the range of possible loop atmospheres. We

discuss the observational data base for this investigation in § II. We describe the model computational techniques and summarize the stellar coronal loop model results in § III. In § IV we discuss the implications of the results, and we present a summary of our conclusions along with suggestions for the directions of future research in § V.

## II. OBSERVATIONS

The transition region line spectra were obtained with the short-wavelength (1175–2000 Å) SWP camera on board the *IUE* satellite. A description of the *IUE* spacecraft and its in-flight performance, including the telescope, spectrographs, and standard data reduction procedures, is given by Boggess *et al.* (1978a, b). The far-ultraviolet observations were acquired through the large aperture in the low-dispersion mode. We reduced the acquired UV spectra utilizing standard *IUE* data reduction techniques. We applied the intensity transfer function given by Bohlin and Holm (1980) for the SWP camera.

In this investigation, we are principally concerned with the observed fluxes of the prominent, optically thin transition region emission lines in the 1200–2000 Å range accessible to *IUE*. These features include the C iv  $\lambda 1550$  resonance doublet, the Si iv–O iv blend at 1400 Å, and the N v  $\lambda 1240$  resonance line. The electron temperatures at which the maximum line emissivities occur (basically corresponding to the maxima of the ionization fractions for the aforementioned ions) for these particular features are approximately  $T_{\text{max}} = 79,000$ , 110,000, and 200,000 K, respectively (J. C. Raymond 1983, private communication). The observed fluxes at the Earth for these transition region lines are given in Table 1. We estimated the errors in the fluxes by inspection of the signal fluctuations near these features. We deduce the error in the observed fluxes to be in the range 20%–30%. The fluxes of the bright emission lines of C iv  $\lambda 1550$  and the 1400 Å Si iv–O iv blend are generally accurate to within 15%–25%, while the error in the weaker N v  $\lambda 1240$  line fluxes are more nearly 25%–35%. These error estimates do not include any systematic errors that may be present in the *IUE* absolute flux scale.

The observed X-ray fluxes and the deduced coronal temperatures, as obtained by the *Einstein Observatory*, for the stars considered here are also listed in Table 1. We emphasize that

TABLE 1  
OBSERVED ULTRAVIOLET AND X-RAY FLUXES

| Object                         | Spectral Type | Si iv–O iv<br>(ergs $\text{cm}^{-2}$ $\text{s}^{-1}$ ) | C iv<br>(ergs $\text{cm}^{-2}$ $\text{s}^{-1}$ ) | N v<br>(ergs $\text{cm}^{-2}$ $\text{s}^{-1}$ ) | X-Ray<br>(ergs $\text{cm}^{-2}$ $\text{s}^{-1}$ ) | $T_{\text{corona}}$<br>(K) |
|--------------------------------|---------------|--|--|---|---|----------------------------|
| Solar minimum .....            | G2 V          | 3.8 (–2) <sup>a</sup>                                  | 1.2 (–1) <sup>a</sup>                            | 8.2 (–3) <sup>a</sup>                           | 2.1 (–1) <sup>b</sup>                             | 1.8 (6) <sup>b</sup>       |
| Solar maximum .....            | G2 V          | 1.1 (–1) <sup>a</sup>                                  | 2.9 (–1) <sup>a</sup>                            | 1.9 (–2) <sup>a</sup>                           | 5.5 (–1) <sup>b</sup>                             | 3 (6) <sup>b</sup>         |
| $\alpha$ Cen B .....           | K1 V          | 8.6 (–13) <sup>a</sup>                                 | 1.1 (–12) <sup>a</sup>                           | 1.9 (–13) <sup>a</sup>                          | 1.3 (–11) <sup>b</sup>                            | 2.1 (6) <sup>b</sup>       |
| $\iota$ Per .....              | G4 V          | 1.9 (–13)  | 1.2 (–13)  | 1.5 (–14)                                       | 1.9 (–13)   | 2.6 (6)                    |
| $\mu$ Her .....                | G5 IV         | 9.4 (–14)  | 2.5 (–13)  | 5.6 (–14)                                       | 6.6 (–13)   | 2.6 (6)                    |
| $\sigma$ Dra .....             | K0 V          | 1.6 (–13)  | 1.7 (–13)  | 4.1 (–14)                                       | 1.4 (–12)   | 2.3 (6)                    |
| HR 3538 .....                  | G3 V          | 4.5 (–14)  | 7.2 (–14)  | 1.8 (–14)                                       | 9.7 (–13)   | 3.1 (6)                    |
| $\epsilon$ Eri .....           | K2 V          | 4.2 (–13) <sup>a</sup>                                 | 1.0 (–12) <sup>a</sup>                           | 1.9 (–13) <sup>a</sup>                          | 1.3 (–11) <sup>c</sup>                            | 3.4 (6) <sup>c</sup>       |
| HD 206860-1 <sup>d</sup> ..... | G0 V          | 1.1 (–13)  | 1.2 (–13)  | 2.1 (–14)                                       | 2.2 (–12) <sup>e</sup>                            | 4.4 (6)                    |
| HD 206860-2 <sup>d</sup> ..... | G0 V          | 1.1 (–13)  | 1.2 (–13)  | 2.1 (–14)                                       | 2.2 (–12) <sup>e</sup>                            | 4.4 (6)                    |
| HD 5303 .....                  | G2 V (+F)     | 1.5 (–13)  | 5.7 (–13)  | 4.5 (–14)                                       | 8.3 (–12) <sup>f</sup>                            | 2.5 (7) <sup>f</sup>       |

<sup>a</sup> Following measured or quoted values from Ayres, Marstad, and Linsky 1981.

<sup>b</sup> From Golub *et al.* 1982a.

<sup>c</sup> Average value determined from data given in Ayres, Marstad, and Linsky 1981 or from this paper.

<sup>d</sup> Multiple ultraviolet observations obtained for this object.

<sup>e</sup> Note that only one X-ray measurement is available for this object.

<sup>f</sup> Average of two measurements.

the X-ray and ultraviolet data given in Table 1 were *not* acquired simultaneously. A description of the in-flight performance of, and instrumentation for, the *Einstein* spacecraft is given by Giacconi *et al.* (1979). The X-ray fluxes displayed in Table 1 were measured with the imaging proportional counter (IPC). The spectral sensitivity of the IPC is nominally 0.2–4 keV. Additional details regarding the instrumentation combined with a discussion of the procedures adopted to finally derive the observed X-ray fluxes are given by Golub *et al.* (1982b).

### III. MODEL COMPUTATIONS AND RESULTS

Following Golub *et al.* (1982a), we envisage a stellar atmosphere consisting of loops of magnetically confined plasma where each loop is subject to the constraint imposed by the RTV scaling law

$$T = 1.4 \times 10^3 (pL)^{1/3}, \quad (1)$$

where  $T$ ,  $p$ , and  $L$  are the coronal temperature, base pressure, and loop semilength, respectively. Equation (1) is applicable to loops which are in hydrostatic equilibrium and which are characterized by lengths  $L \leq s_p$ , where  $s_p$  is the local coronal pressure scale height. As shown by Serio *et al.* (1981), equation (1) requires modification by a multiplicative term for loops characterized by lengths  $L \leq s_p$ , or

$$T = 1.4 \times 10^3 (p_0 L)^{0.33} \exp[-0.04L(2/s_H + 1/s_p)], \quad (2)$$

where  $p_0$  is the base pressure of the loop and  $s_H$  is the energy deposition scale height of the presumed magnetic field-related nonradiative heating occurring within the loop. The relations (1) and (2) essentially divide coronal loops into two classes, namely, those loops which are entirely filled with emitting plasma and those for which the exponential decline in plasma density becomes significant.

The construction of the stellar coronal loop atmospheric models we present here relies upon several assumptions, the applicability of which has been verified by previous solar work. In particular, we assume that (1) the transition region of a solar-type star is a geometrically thin, constant pressure interface between the stellar chromosphere and corona and thus constitutes the base of the stellar corona, in analogy to the solar transition region, (2) the loops are in hydrostatic equilibrium, (3) a single temperature component produces the observed coronal emission, (4) the loop cross section is constant with height, (5) the heating in the loop is uniform (with respect to volume), and (6) the loops are all identical. The first assumption of a geometrically thin transition region analogous to the solar transition region is corroborated by the results of Ayres and Linsky (1980). These investigators find that models of the transition regions of  $\alpha$  Cen A and B are quantitatively similar to that of the solar transition region. The second assumption follows Serio *et al.* (1981), who employed static modeling, since active and quiet solar loop structures are observed to be relatively quiescent on typical cooling time scales. The third assumption is less certain, especially in view of the previously described results of Swank *et al.* (1981), who find evidence for two-component X-ray emission from RS CVn systems. A determination of the presence and nature of an additional X-ray-emitting high-temperature (active) component on solar-type stars from *Einstein* IPC data alone will require the development of a more refined technique for IPC data analysis that is beyond the scope of this investigation. We

thus defer consideration of multicomponent stellar coronae to a future, more comprehensive investigation (Vaiana *et al.* 1985).

Our use of loop models characterized by loops of constant cross section and uniform heating is based on the results of the detailed calculations by Withbroe (1978) and Serio *et al.* (1981), who investigated the effects of varying  $s_H$  and loop expansion parameters (see also Vesecky, Antiochos, and Underwood 1979). Serio *et al.* (1981) find that the inclusion of flux-tube expansion in the transition region between the temperatures  $7 \times 10^5$  K and  $10^6$  K has a negligible effect on the loop temperature and pressure profile; the only noticeable effect is a slight increase in differential emission measure in this temperature range. Withbroe (1978) finds that the scaling law relating loop temperature, pressure, and length for a loop in which the energy is deposited at the top, rather than uniformly distributed over the loop volume, is nearly identical with the RTV scaling law. In basic summary, derived stellar coronal parameters do not sensitively depend on the effects arising from flux-tube expansion and heating scale height (see also Pallavicini *et al.* 1981; Peres *et al.* 1982; Schmitt *et al.* 1985), with the exception noted by RTV and Serio *et al.* (1981), namely, that short ( $s_H \ll s_p$ ) energy deposition scale heights result in unstable loop configurations. The last assumption is a necessary simplification which reflects the lack of direct observational data concerning the distribution in geometrical scales of the stellar outer atmosphere. Finally, we emphasize that the observed UV fluxes only determine the emission measure at  $T \sim 10^5$  K; a determination of electron densities and pressures requires the formulation of density-sensitive line ratios that are not available in our data set.

The observational constraints that a model must satisfy include the derived value of the coronal temperature, assumed to be equal to the maximum loop temperature,<sup>5</sup> which, in turn, occurs at the top of the loop (RTV), and the observed ultraviolet line fluxes combined with the soft X-ray flux. We adopt the theoretical constraints outlined by Pallavicini *et al.* (1981) for the static stellar loop models we construct in this investigation. In particular, we impose an energy balance requirement of the form

$$E_R(s) + E_H(s) = \text{div } F_c(s), \quad (3)$$

where  $E_R = -N_e^2 P(T)$  represents radiative losses,  $E_H$  is the energy deposited in the loop, and  $F_c$  is the conductive flux parallel to the magnetic field (Pallavicini *et al.* 1981). In accord with the application of the RTV scaling law, we require that the conductive flux vanish at the loop footpoints (RTV; Serio *et al.* 1981).

In order to compute the emergent UV line fluxes and the broad-band X-ray emission from a loop, we utilize a numerical code developed by Serio *et al.* (1981). In particular, the flux of an effectively thin, collisionally excited transition region spectral line formed under conditions of coronal equilibrium (Thomas 1965) is given by (Pottasch 1963; Withbroe 1975; Pallavicini *et al.* 1981)

$$F = 1.75 \times 10^{-16} A f g_{\text{eff}} \int_T Q(T) G(T) dT, \quad (4)$$

<sup>5</sup> We note that, as discussed by Schmitt *et al.* (1985), some error will be introduced in this approach, since the coronal temperature derived from IPC observations is weighted by the stellar coronal emission measure distribution, the plasma cooling function, and the instrument response. Thus the inferred temperature really corresponds to a coronal "effective temperature" that would, in general, be less than the temperature at the top of a loop.

where  $F$  is the total line flux,  $A$  is the elemental abundance relative to hydrogen,  $f$  is the oscillator strength of the line or the effective oscillator strength of an unresolved multiplet,  $g_{eff}$  is the effective Gaunt factor, and  $G(T)$  is a temperature-dependent function that describes the excitation and ionization properties of the atom producing the line. The function  $Q(T)$  is the differential emission measure defined by (Withbroe 1975, 1978; Pallavicini *et al.* 1981)

$$Q(T) = N_e^2 (dT/dh)^{-1} \text{ cm}^{-5} \text{ K}^{-1}, \quad (5)$$

where  $N_e$  is the electron density and  $h$  is a coordinate along the line of sight. The functions  $G(T)$  and  $Q(T)$  are estimated from the results of the ionization equilibrium and line emissivity calculations of Raymond and Doyle (1981). The results obtained by Raymond and Doyle (1981) are appropriate for regions where  $N_e \sim 10^{10} - 10^{11} \text{ cm}^{-3}$ . We consider these kinds of densities to be representative of the enhanced pressures that characterize solar and stellar active regions. We note that the ionization equilibrium calculations of Jordan (1969) are valid for low-density ( $N_e < 10^9 \text{ cm}^{-3}$ ) plasmas that are likely more representative of the conditions in the quiet Sun exterior to coronal loop structures.

Gaunt factors and oscillator strengths for the lines considered here are given by Wiese, Smith, and Miles (1969), Burton *et al.* (1971), and Dupree (1972). We adopted the solar abundances presented by Withbroe (1976) as quoted by Raymond and Doyle (1981, their Table 1). We reduced the observed flux of the Si IV–O IV blend by 30% in order to achieve a more accurate comparison between our model predictions of the Si IV  $\lambda 1400$  line flux and the observations. The percentage contribution of Si IV to the Si IV–O IV blend was empirically ascertained from solar data acquired by the *Skylab* ATM Experiment (Cohen 1981). The total line fluxes are computed on the basis of the static loop model that is finally derived. The same procedure also applies to the computation of the broad-band soft X-ray emission. In particular, we utilized the coronal radiative loss function for an optically thin plasma of solar abundances as calculated by J. C. Raymond and tabulated by RTV.

We compute the filling factor of identical loops that is required to yield the observed emission by comparing the emission from a single loop to the observed UV and X-ray fluxes. More specifically, we solve for the value of the filling factor that minimizes the sum of the squares of the logarithmic differences between the observed and computed values of the UV and X-ray fluxes. The “best-fit” model (or models) was determined by an intercomparison of a computed grid of models in the  $(p, f)$ -plane combined with our subjective assessment of the overall quality of the agreement between the model predictions and the actual ultraviolet and X-ray data available for a given star. As an illustrative example, we display a sequence of possible models for  $\mu$  Her in Figure 1. The computational results for  $\mu$  Her, as shown in Figure 1, reveal that acceptable fits to the data (that are within the observational errors) are achieved for loop filling factors in the range  $0.09 \leq f \leq 0.38$  and loop base pressures between about 0.25 and  $1.0 \text{ dyne cm}^{-2}$ . Lower loop pressures yield unrealistic filling factors and X-ray fluxes that are less than the observed fluxes, even with filling factors greater than unity. Loop model atmospheres characterized by significantly higher pressures and lower loop filling factors can yield the observed X-ray flux of  $\mu$  Her, but these models consistently underpredict the UV transition region line emissions.

The static loop model itself is obtained through an iterative procedure. We initially select a coronal base pressure (corresponding to the transition region pressure) and loop length that, according to the RTV scaling law (eq. [1]), yield the observed coronal temperature listed in Table 1. The procedure used to construct static loop models is based on the simple fact that in equilibrium, the total heat input into the loop must equal the total radiative losses from the loop (thermal conduction only serves to redistribute heat within a loop); if this equality is satisfied, then the conductive flux at the loop apex will vanish (the conductive flux at the loop base is always assumed to be negligible in our models). Thus, we begin with a trial temperature-density distribution with a loop of fixed dimensions and fixed base pressure, determine where along the loop the conductive flux vanishes (in addition to the zero at the loop footpoint), and then iteratively adjust the spatially uniform heating rate until the conductive flux vanishes at the loop apex. In this way, we determine the equilibrium solution to the loop atmosphere problem for fixed base pressure and loop length. The radiative emission from a single loop is subsequently computed and the filling factor of identical loops is finally determined on the basis of the observed UV and X-ray fluxes, and the model predictions of these quantities, as previously outlined.

We delineate in Table 2 the stellar parameters we adopt for each object considered in this investigation. We derive the stellar surface gravity from the spectral type and the corresponding mass and radius estimates given by Allen (1976). In some cases we deduce the stellar radius from the  $(V - R)$ -angular diameter relations determined by Barnes and Evans (1976) and Barnes, Evans, and Parsons (1976) for those stars in our sample for which measured  $(V - R)$  colors are available. Stellar distances follow from the parallax measurements tabulated by Gliese (1969), with the exception of HD 5303. In the case of this star, we estimate the distance from its spectral type and apparent magnitude (Seward and Mitchell 1981). Moreover, we assume that the primary emitter in this RS CVn system is the later type G2 V star. Furthermore, either multiple UV or multiple X-ray observations are available for some objects. In these instances we adopt the mean X-ray flux (and mean  $T_{\text{corona}}$ ) for the comparison of the model predictions with the observations for HD 206860 separately in order to examine the potential effects of both intrinsic stellar atmospheric variability and the lack of simultaneously acquired X-ray and UV data for the sample of stars considered in this investigation.

We list the loop model parameters that best fit the observational data for the objects considered here in the final three columns of Table 2. The fourth column is a list of the maximum loop temperatures, which are, in turn, identified as the stellar coronal temperatures. We display in Figures 1 and 2 examples of the comparisons between the predictions of the emission from static loop atmospheres and the observations.

We display in Figure 3 the distribution of the emission coefficients with distance  $s$  along the loop for the spectral bands considered in this investigation. The particular loop model shown corresponds to the solar maximum model with  $p = 1.50 \text{ dynes cm}^{-2}$  (cf. Fig. 2). Inspection of Figure 3 reveals that the locations of the maxima of the transition region lines are located two orders of magnitude lower in the atmosphere than the maximum of the coronal soft X-ray (*HEAO 2*) emission. We mention this in order to emphasize that observed X-ray emission is the only *direct* diagnostic of coronal plasma ( $T \geq 10^6$

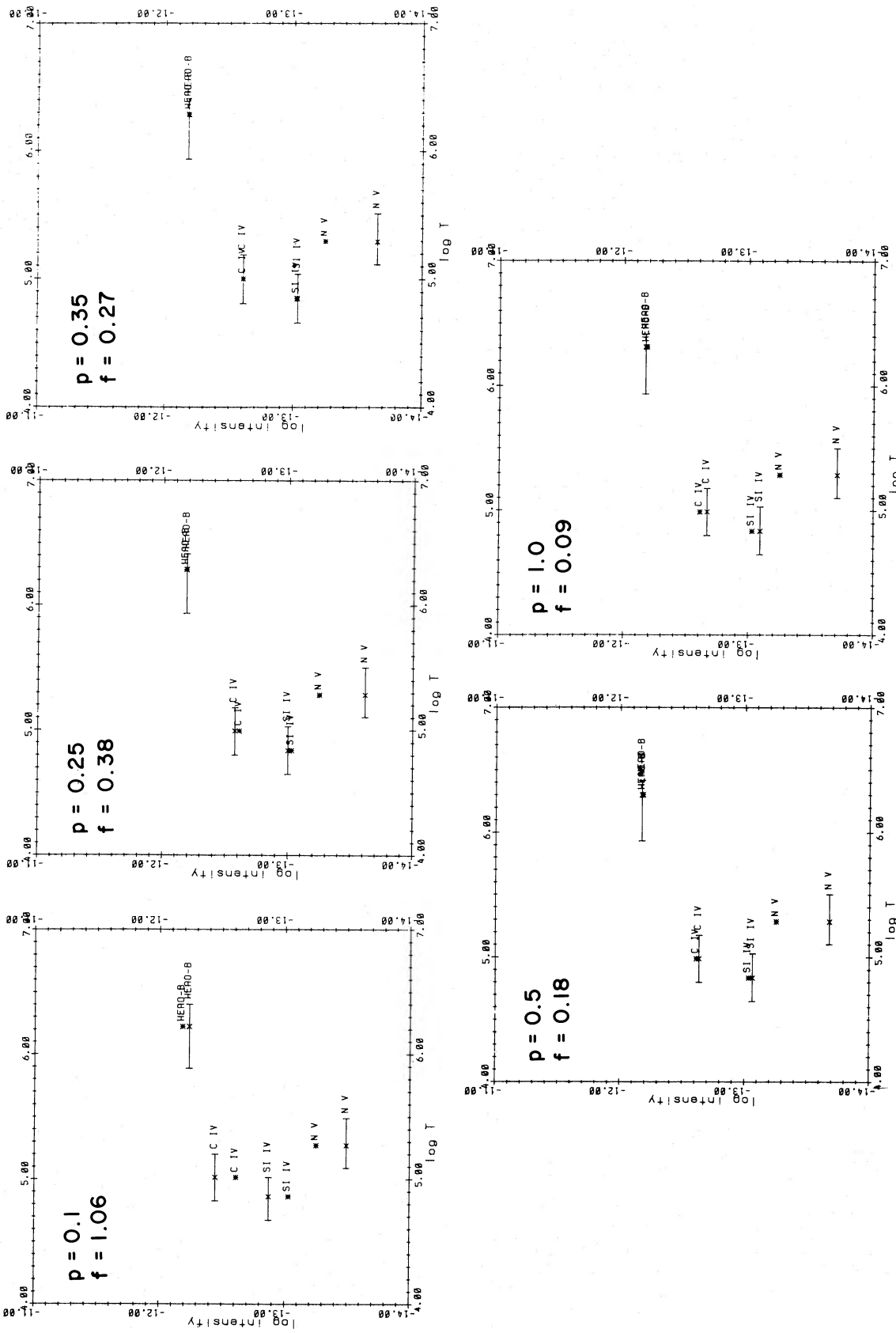


FIG. 1—A grid of possible coronal loop model atmospheres in the  $(p, f)$ -plane for  $\mu$  Her. The observed values are noted by asterisks, while the computed values are designated by crosses. See text for discussion.

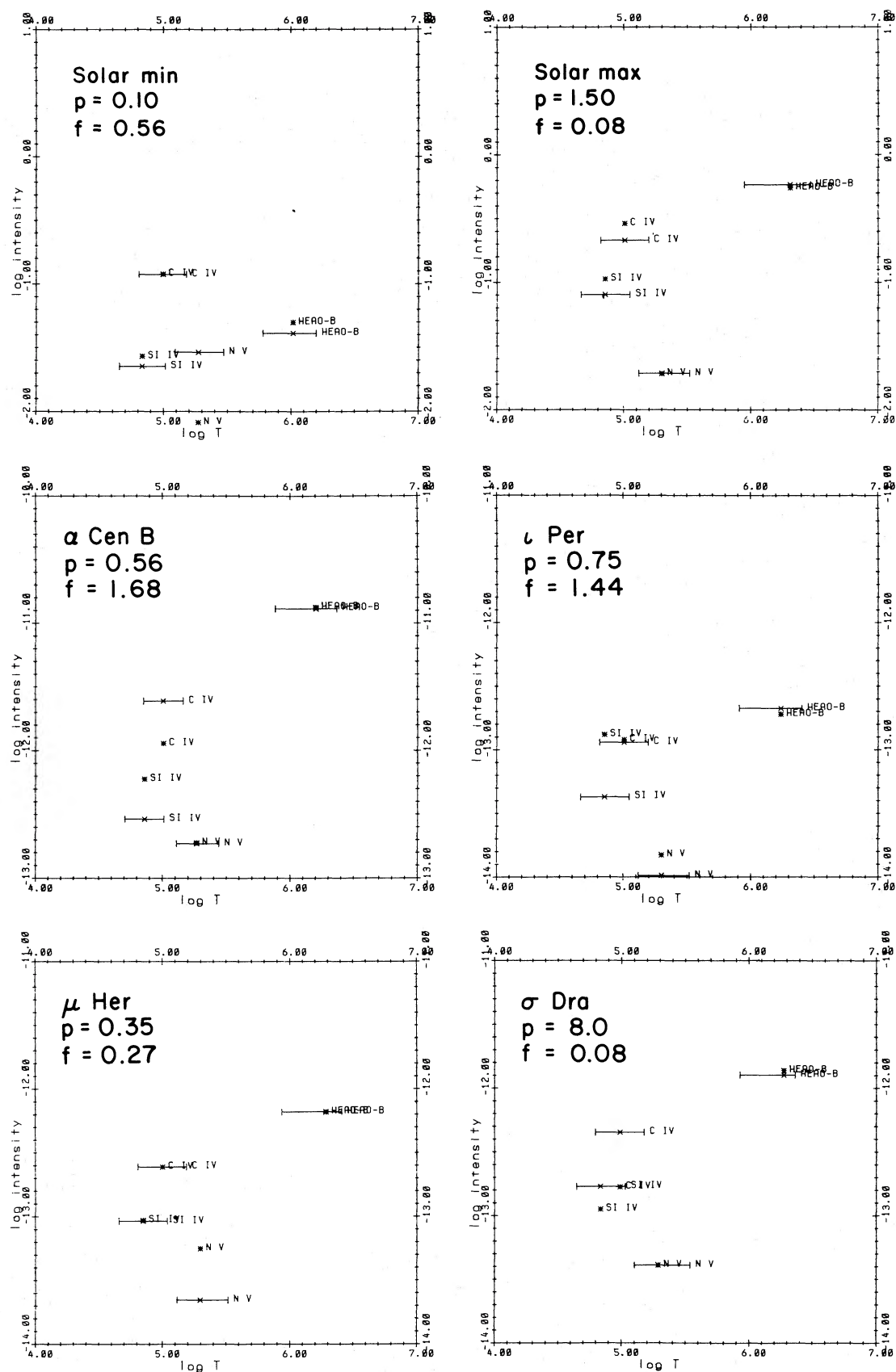


FIG. 2.—Examples of the computed values of the transition region and soft X-ray coronal emissions versus electron temperature for the best-fit stellar coronal loop atmospheric models discussed in this investigation. The observed values are noted by an asterisk. The computed values are designated by crosses located at the temperature of maximum volume emissivity, while the bars extend over the temperature range in which the volume emissivity is greater than  $1/e$  of the corresponding maximum value.

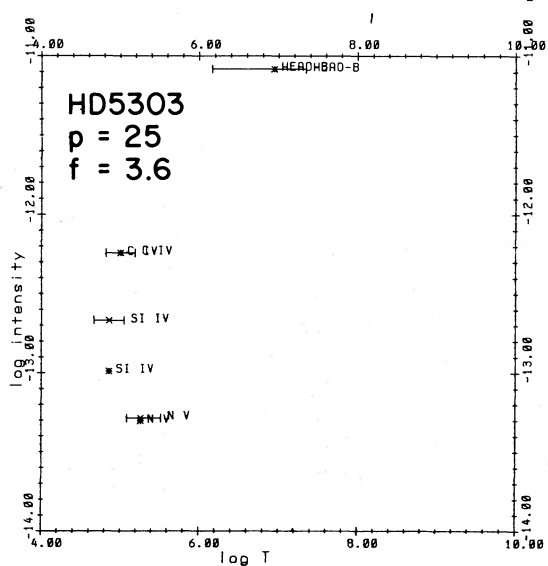
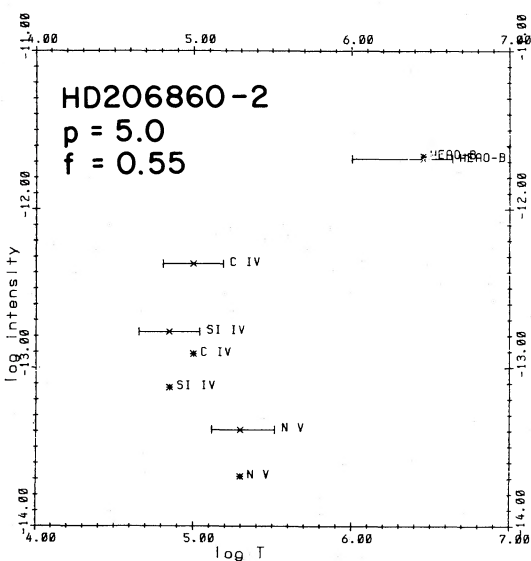
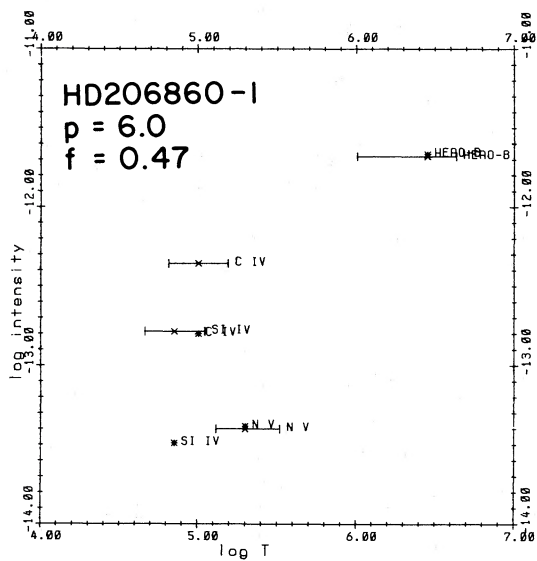
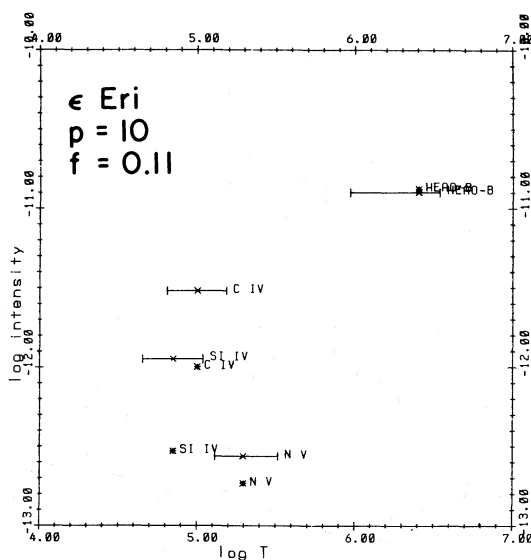
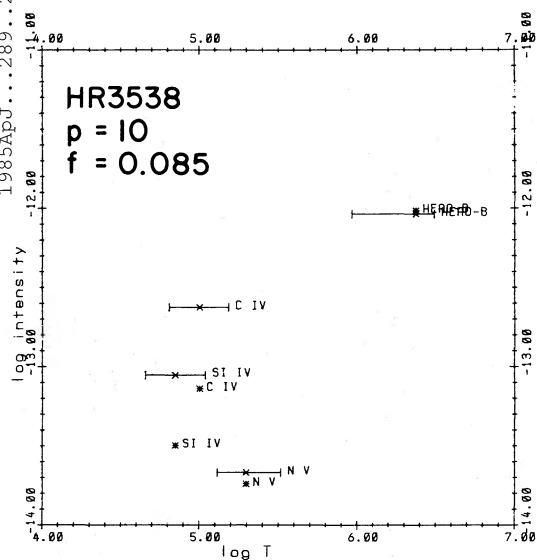


FIG. 2—(continued)

TABLE 2  
STELLAR ATMOSPHERIC LOOP MODEL PARAMETERS

| Object                                   | $g$<br>( $\text{cm s}^{-2}$ ) | $d$<br>(pc) | $R/R_{\odot}$ | $T_{\text{max}}$<br>(K) | $p$<br>( $\text{dynes cm}^{-2}$ ) | $f$        | $L$<br>(cm)     |
|--|-------------------------------|-------------|---------------|-------------------------|-----------------------------------|------------|-----------------|
| Solar minimum (G5 V) .....               | 2.75 (4)                      | 4.848 (-6)  | 1             | 2.5 (6)                 | 0.10                              | 0.56       | 7.0 (10)        |
| Solar maximum (G2 V) .....               | 2.75 (4)                      | 4.848 (-6)  | 1             | 3.0 (6)                 | 1.50                              | 0.03       | 6.9 (9)         |
| $\alpha$ Cen B (K1 V) .....              | 3.23 (4)                      | 1.34        | 0.87          | 2.4 (6)                 | 0.56                              | 1.68       | 9.5 (9)         |
| $\iota$ Per (G4 V) .....                 | 2.91 (4)                      | 11.6        | 0.95          | 2.6 (6)                 | 0.65-0.85                         | 1.25-1.69  | 7.5 (9)-9.8 (9) |
| $\mu$ Her (G5 IV) .....                  | 5.06 (3)                      | 8.06        | 3.10          | 2.6 (6)                 | 0.35                              | 0.27       | 1.8 (10)        |
| $\sigma$ Dra (K0 V) <sup>a</sup> .....   | 2.95 (4)                      | 5.68        | 0.85          | 2.3 (6)                 | 4.0-16.0                          | 0.04-0.16  | 2.8 (8)-1.1 (9) |
| HR 3538 (G3 V) <sup>a</sup> .....        | 2.88 (4)                      | 11.8        | 0.98          | 3.2 (6)                 | 5.0-10.0                          | 0.085-0.17 | 1.1 (9)-2.2 (9) |
| $\epsilon$ Eri (K2 V) <sup>a</sup> ..... | 3.08 (4)                      | 3.31        | 0.82          | 3.5 (6)                 | 5.0-20.0                          | 0.54-0.22  | 7.5 (8)-3.0 (9) |
| HD 206860-1 <sup>b</sup> (G0 V) .....    | 2.75 (4)                      | 17.5        | 1.05          | 4.4 (6)                 | 6.0-8.0                           | 0.35-0.47  | 3.8 (9)-5.0 (9) |
| HD 206860-2 <sup>b</sup> (G0 V) .....    | 2.75 (4)                      | 17.5        | 1.05          | ...                     | ...                               | ...        | ...             |
| HD 5303 (G2 V + F) .....                 | 2.75 (4)                      | 66          | 1.0           | 24 (6)                  | 25.0                              | 3.64       | 2.2 (1)         |

<sup>a</sup> The quoted range of loop model parameters is applicable in the regime where the model transition region densities are required to be less than  $10^{12} \text{ cm}^{-3}$ . In general, no unique, well-constrained models that satisfy both the far-UV and X-ray data could be determined.

<sup>b</sup> Multiple ultraviolet observations available for this object. See Table 1.

K), while the UV lines are purely transition region diagnostics ( $T \sim 10^5 \text{ K}$ ) formed at the base of a stellar corona. Thus an acceptable semiempirical, single-component stellar coronal loop atmospheric model must correctly predict the observed X-ray emission, since the X-ray flux is the only available diagnostic of regions at coronal temperatures. Transition region line emission *alone* cannot be confidently utilized in the development of self-consistent stellar coronal loop models, since these features are not direct diagnostics of plasma at temperatures  $T \geq 10^6 \text{ K}$  (compare Brown and Jordan 1981; see Schmitt *et al.* 1984). We therefore regard the stellar coronal loop models we construct in this investigation as atmospheric models that attempt simultaneously to account for both the observed transition region line emission and the coronal X-ray emission in a fully self-consistent manner.

#### IV. DISCUSSION

We present in Table 2 the range of  $(p, f)$ -values that "best fit" (according to the previously described method) both the far-ultraviolet and the X-ray data for the solar-type stars con-

sidered in this investigation. Examination of Table 2 and Figure 2 reveals that the model approach adopted herein yields mixed results. For example, the models corresponding to the solar minimum and solar maximum cases fit the data, to within the observational errors, with reasonable values of loop pressure and filling factor. As expected, the solar minimum case is best fit by low-pressure, large-scale loops with a filling factor near unity; the solar maximum observations are best fit by higher pressure, compact loops with lower filling factors. The best-fit models for  $\alpha$  Cen B and  $\iota$  Per do not satisfy *all* the radiative diagnostics. Agreement between the X-ray emission and one of the UV lines is achieved, but the model predictions for the remaining transition region lines are not in accord with the data to within the errors. Moreover, the filling factors for both best-fit models are slightly greater than unity and therefore may be physically unrealistic.

In the cases of  $\sigma$  Dra, HR 3538, and  $\epsilon$  Eri, the models exhibit a systematic overprediction of the UV line emissions. We found that significantly higher pressure loops (i.e., values of  $p$  that were from one to nearly three orders of magnitude higher than those shown in Fig. 2) combined with filling factors of  $f \ll 1$  could equally satisfy the observational data to within the same errors. However, these kinds of loops were characterized by transition region densities  $N_{\text{TR}} \sim 10^{13}-10^{14} \text{ cm}^{-3}$ . Such densities are more nearly photospheric (e.g., see Vernazza, Avrett, and Loeser 1981), although densities of this order of magnitude can be attained during intense flare events. In fact, Walter, Gibson, and Basri (1983) deduce loop pressures in the coronae of the AR Lac system that are similar to those found in small solar flares. Nevertheless, the problem of assigning a unique loop model atmosphere on the basis of the data still remains for these program stars. We note, parenthetically, that low-pressure ( $p < 1$ ) loop atmosphere models can be constructed that predict the observed transition region line emission, but the filling factors are unphysical ( $f \gg 1$ ) and these models tend to underpredict the X-ray emission by factors  $\gtrsim 10$ .

Finally, the model atmosphere for the assumed primary emitter in the RS CVn system HD 5303 is characterized by high-pressure loop structures with loop lengths  $L > R$  and a filling factor  $f > 1$ . Both Swank *et al.* (1981) and Walter *et al.* (1980) find similar results in their investigations of RS CVn systems within the context of loop model atmospheres. The inferred loop length  $L > R$  can be attributed to the high

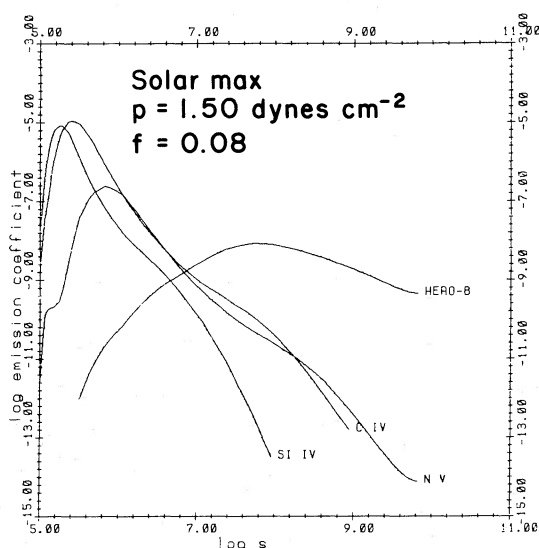


FIG. 3.—The distribution of the emission coefficients with distance  $s$  along a loop for the solar maximum model characterized by  $p = 1.50 \text{ dynes cm}^{-2}$ . See § III for a discussion.

coronal temperature ( $T_{\text{corona}} = 2.5 \times 10^7$ ; see Table 1) combined with a consideration of the RTV scaling law (eq. [1]). Thus the inferred filling factor is more representative of a volume, rather than surface, filling factor of emitting loops. Additional evidence of these kinds of loop structures is given by Simon, Linsky, and Schiffer (1980) in the specific case of the RS CVn system UX Ari. In brief summary, we attained satisfactory fits to the data with loop models characterized by relatively unique, plausible stellar coronal parameters for some stars. This category includes  $\mu$  Her, HD 5303, and the solar minimum and maximum cases, respectively. However, the results for the remaining stars are less satisfactory in self-consistently accounting for the observed far-UV and X-ray emission.

Given the mixed results achieved in our attempt to construct relatively unique, semiempirical loop model atmospheres that satisfy both the UV and the X-ray data, it becomes necessary to examine the possible origins of the discrepancies between the model predictions and the observations. For example, we obtained models that satisfactorily predicted the observed X-ray emission and partially accounted for the initial UV observations for HD 206860 (designated HD 206860-1 in Table 2 and Fig. 2). However, no acceptable model could account for both the X-ray emission and the second set of UV observations acquired for this star (designated HD 206860-2 in Table 2 and Fig. 2). More specifically, all models that correctly predicted the X-ray emission consistently *overpredicted* the UV emission in all lines. Models characterized by low-pressure loops correctly predicted the UV emission of HD 206860-2, but they underpredicted the X-ray emission by at least an order of magnitude. These low-pressure models were further characterized by physically unrealistic filling factors of  $f \gg 1$ . Inspection of Table 1 reveals that the transition region UV emission of the initial observation of HD 206860 (HD 206860-1) is enhanced relative to the later observation (HD 206860-2). Thus the single measurement of the X-ray emission from the star must be more compatible with the relatively enhanced transition region of HD 206860-1 than with that of the later observation of this object. We note that the loop model atmospheres for HR 3538 and  $\epsilon$  Eri also overpredict the UV emission (see Fig. 2). We therefore suggest on the basis of the results for HD 206860 that intrinsic stellar variability can contribute to the discrepancies between the observations and the model predictions for the stars considered in this investigation. Conversely, the success of the loop models (in terms of predicting all of the observed UV and X-ray data to within the errors) constructed for the solar case is likely due to the fact that the UV measurements are known to correspond to the quoted soft X-ray measurements at each of two phases in the solar cycle.

In addition to intrinsic transition region and coronal stellar variability, the presence of a hard component ( $T_{\text{corona}} \gtrsim 10^7$  K) which can contribute at least half the emission measure in the observed soft X-ray emission (e.g., Swank *et al.* 1981) will inevitably lead to discrepancies and uniqueness problems in a single-component model approach. Furthermore, we note that while sites of X-ray emission on the Sun always coincide with

underlying sites of UV transition region emission, sites of far-UV emission do not always correspond to sites of coronal X-ray emission. For example, large, "cool loops" characterized by a high EUV line luminosity, but no X-ray emission, are observed in the vicinity of sunspots (Foukal 1975; Raymond and Foukal 1982). Finally, there may be a significant contribution to far-UV emission by network, while the soft X-ray emission originates predominantly from active regions, at least in the case of active stars, following the solar analogy (cf. Golub 1982). In low-activity stars, a combination of network and large-scale, evolved structures would be expected to dominate the contributions to observed UV and soft X-ray emission. Clearly, if this phenomenon is present on the surfaces of solar-type stars, then it would again be manifested, in part, through discrepancies between the observations and the predictions of single-component loop models.

#### V. SUMMARY

We have sought to constrain the range of possible coronal loop model atmospheres, as applied to interpret stellar observations, through the addition of nonsimultaneously acquired *IUE* ultraviolet transition region line emission data to previously obtained *Einstein* IPC soft X-ray observations. We find that the addition of these UV data alone is not sufficient, in most cases, to provide well-constrained, relatively unique models of stellar coronae and transition regions characterized by plausible parameters in the pressure-filling factor plane (see also Schmitt *et al.* 1985). We tentatively attribute the origins of the discrepancies between the model predictions and the observations to (1) the effects of stellar coronal and transition region variability, (2) the presence of multiple coronal components, and (3) the possibility that, as on the Sun, there is not always a one-to-one correspondence between sites of transition region UV and coronal soft X-ray emission.

The results of this investigation suggest that the applicability of coronal loop models to stars can be rigorously examined only through the acquisition of simultaneous ultraviolet and moderate ( $E/\Delta E \sim 100$ ) spectral resolution X-ray observations. Moderate resolution X-ray spectroscopy is necessary in order to distinguish between multiple coronal components. Furthermore, observations of active, eclipsing systems in this mode (e.g., Walter, Gibson, and Basri 1983) can potentially yield geometrical scales for the plasma emission, thus providing an invaluable model constraint.

We acknowledge interesting and valuable discussions with R. Rosner concerning the results presented in this study. We also acknowledge valuable discussions with J. Raymond. We are grateful to J. Linsky for his critical comments on an earlier version of this manuscript. We also acknowledge the support of the Ministero Pubblica Istruzione and the Piano Spaziale Nazionale of Italy. Finally, we acknowledge support for this investigation as provided by NASA grants NAG 5-87 and NAGW-112 to the Smithsonian Astrophysical Observatory and by the Visitors Program of the Smithsonian Institution (M. S. G., G. P., and S. S.).

#### REFERENCES

- Allen, C. W. 1976, *Astrophysical Quantities* (3d ed. London: Athlone).  
 Ayres, T. R., and Linsky, J. L. 1980, *Ap. J.*, **235**, 76.  
 Ayres, T. R., Marstad, N. C., and Linsky, J. L. 1981, *Ap. J.*, **247**, 545.  
 Barnes, T. G., and Evans, D. S. 1976, *M.N.R.A.S.*, **174**, 489.  
 Barnes, T. G., Evans, D. S., and Parson, S. B. 1976, *M.N.R.A.S.*, **174**, 503.  
 Boggess, A., *et al.* 1978a, *Nature*, **275**, 372.  
 ———, 1978b, *Nature*, **275**, 377.  
 Bohlin, R. C., and Hom, A. V. 1980, *NASA IUE Newsletter*, No. 10, p. 37.  
 Brown, A., and Jordan, C. 1981, *M.N.R.A.S.*, **196**, 757.  
 Burton, W. M., Jordan, C., Ridgeley, A., and Wilson, R. 1971, *Phil. Trans. Roy. Soc. London, A*, **278**, 81.  
 Cohen, L. 1981, *An Atlas of Solar Spectra between 1175 and 1950 Angstroms Recorded on Skylab with the NRL's Apollo Telescope Mount Equipment* (NASA Reference Pub. 1069; Washington, D.C.: Government Printing Office).  
 Dupree, A. K. 1972, *Ap. J.*, **178**, 527.

- Foukal, P. 1975, *Solar Phys.*, **43**, 327.  
 Giacconi, R., et al. 1979, *Ap. J.*, **230**, 540.  
 Gliese, W. 1969, *Catalogue of Nearby Stars* (Heidelberg: G. Braun).  
 Golub, L. 1982, in *Cool Stars, Stellar Systems and the Sun*, ed. M. S. Giampapa and L. Golub (*Smithsonian Ap. Obs. Spec. Rept.*, No. 392), p. 39.  
 Golub, L., Harnden, F. R., Jr., Pallavicini, R., Rosner, R., and Vaiana, G. S. 1982a, *Ap. J.*, **253**, 242.  
 Golub, L., Poletto, G., Noci, G., and Vaiana, G. S. 1982b, *Ap. J.*, **259**, 359.  
 Ionson, J. A. 1978, *Ap. J.*, **226**, 650.  
 Jordan, C. 1969, *M.N.R.A.S.*, **142**, 501.  
 Pallavicini, R., Peres, G., Serio, S., Vaiana, G. S., Golub, L., and Rosner, R. 1981, *Ap. J.*, **247**, 692.  
 Peres, G., Rosner, R., Serio, S., and Vaiana, G. S. 1982, *Ap. J.*, **252**, 791.  
 Pottash, S. R. 1963, *Ap. J.*, **137**, 945.  
 Radick, R. R., et al. 1983, *Pub. A.S.P.*, **95**, 300.  
 Raymond, J. C., and Doyle, J. G. 1981, *Ap. J.*, **245**, 1141.  
 Raymond, J. C., and Foukal, P. 1982, *Ap. J.*, **253**, 323.  
 Rosner, R., Golub, L., Coppi, B., and Vaiana, G. S. 1978, *Ap. J.*, **222**, 317.  
 Rosner, R., Tucker, W. H., and Vaiana, G. S. 1978, *Ap. J.*, **220**, 643 (RTV).  
 Rosner, R., and Vaiana, G. S. 1977, *Ap. J.*, **216**, 141.  
 Schmitt, J. H. M. M., Harnden, F. R., Jr., Peres, G., Rosner, R., and Serio, S. 1985, *Ap. J.*, **288**, 751.  
 Serio, S., Peres, G., Vaiana, G. S., Golub, L., and Rosner, R. 1981, *Ap. J.*, **243**, 288.  
 Seward, F. D., and Mitchell, M. 1981, *Ap. J.*, **243**, 736.  
 Simon, T., Linsky, J. L., and Schiffer, F. H., III. 1980, *Ap. J.*, **239**, 911.  
 Swank, J. H., White, N. E., Holt, S. S., and Becker, R. H. 1981, *Ap. J.*, **246**, 208.  
 Thomas, R. N. 1965, *Some Aspects of Nonequilibrium Thermodynamics in the Presence of a Radiation Field* (Boulder: University of Colorado Press).  
 Vaiana, G. S., et al. 1981, *Ap. J.*, **245**, 163.  
 ———. 1985, in preparation.  
 Vaiana, G. S., and Rosner, R. 1978, *Ann. Rev. Astr. Ap.*, **16**, 393.  
 Van Speybroeck, L. P., Krieger, A. S., and Vaiana, G. S. 1970, *Nature*, **227**, 818.  
 Vaughan, A. H., Balivas, S. L., Middlekoop, F., Hartmann, L., Mihalas, D., Noyes, R. W., and Preston, G. W. 1981, *Ap. J.*, **250**, 276.  
 Vernazza, J. E., Avrett, E. H., and Loeser, R. 1981, *Ap. J. Suppl.*, **45**, 635.  
 Vesecky, J. F., Antiochos, S. K., and Underwood, J. H. 1979, *Ap. J.*, **233**, 987.  
 Walter, F. M., Cash, W., Charles, P. A., and Bowyer, C. S. 1980, *Ap. J.*, **236**, 212.  
 Walter, F. M., Gibson, D. M., and Basri, G. S. 1983, *Ap. J.*, **267**, 665.  
 Wiese, W. L., Smith, M. W., and Miles, B. M. 1969, *Atomic Transition Probabilities*, Vol. 2 (Washington, D.C.: NBS).  
 Wilson, O. C. 1978, *Ap. J.*, **226**, 379.  
 Withbroe, G. L. 1975, *Solar Phys.*, **45**, 301.  
 ———. 1976, paper presented at annual meeting of the American Geophysical Union.  
 ———. 1978, in *Proc. OSO 8 Workshop* (Boulder: University of Colorado Press), p. 2.

MARK S. GIAMPAPA: National Solar Observatory, 950 N. Cherry Avenue, P.O. Box 26732, Tucson, AZ 85726

LEON GOLUB, GIOVANNI PERES, SALVATORE SERIO, and GIUSEPPE S. VAIANA: Harvard-Smithsonian Center for Astrophysics; 60 Garden Street, Cambridge, MA 02138